



# Micro/Nanostructured Topography on Titanium Orchestrates Dendritic Cell Adhesion and Activation via $\beta$ 2 Integrin-FAK Signals

Yang Yang<sup>1,2,\*</sup>, Yujing Lin<sup>1,2,\*</sup>, Ruogu Xu<sup>1,2</sup> , Zhengchuan Zhang<sup>1,2</sup>, Wenyi Zeng<sup>1,2</sup>, Qiong Xu<sup>1,2</sup>, Feilong Deng<sup>1,2</sup> 

<sup>1</sup>Department of Oral Implantology, Guanghua School of Stomatology, Hospital of Stomatology, Sun Yat-Sen University, Guangzhou, People's Republic of China; <sup>2</sup>Guangdong Provincial Key Laboratory of Stomatology, Guangzhou, People's Republic of China

\*These authors contributed equally to this work

Correspondence: Qiong Xu; Feilong Deng, Department of Oral Implantology, Hospital of Stomatology, Guanghua School of Stomatology, Sun Yat-Sen University, No. 56, Ling Yuan Xi Road, Guangzhou, 510055, People's Republic of China, Tel +86 20 83862537, Fax +86 20 83822807, Email xqiong@mail.sysu.edu.cn; dengfl@mail.sysu.edu.cn

**Background and Purpose:** In clinical application of dental implants, the functional state of dendritic cells (DCs) has been suggested to have a close relationship with the implant survival rate or speed of osseointegration. Although microscale surfaces have a stable osteogenesis property, they also incline to trigger unfavorable DCs activation and threaten the osseointegration process. Nanoscale structures have an advantage in regulating cell immune response through orchestrating cell adhesion, indicating the potential of hierarchical micro/nanostructured surface in regulation of DCs' activation without sacrificing the advantage of microscale topography.

**Materials and Methods:** Two micro/nanostructures were fabricated based on microscale rough surfaces through anodization or alkali treatment, the sand-blasted and acid-etched (SA) surface served as control. The surface characteristics, in vitro and in vivo DC immune reactions and  $\beta$ 2 integrin-FAK signal expression were systematically investigated. The DC responses to different surface topographies after FAK inhibition were also tested.

**Results:** Both micro/nano-modified surfaces exhibited unique composite structures, with higher hydrophilicity and lower roughness compared to the SA surface. The DCs showed relatively immature functional states with round morphologies and significantly downregulated  $\beta$ 2 integrin-FAK levels on micro/nanostructures. Implant surfaces with micro/nano-topographies also triggered lower levels of DC inflammatory responses than SA surfaces in vivo. The inhibited FAK activation effectively reduced the differences in topography-caused DC activation and narrowed the differences in DC activation among the three groups.

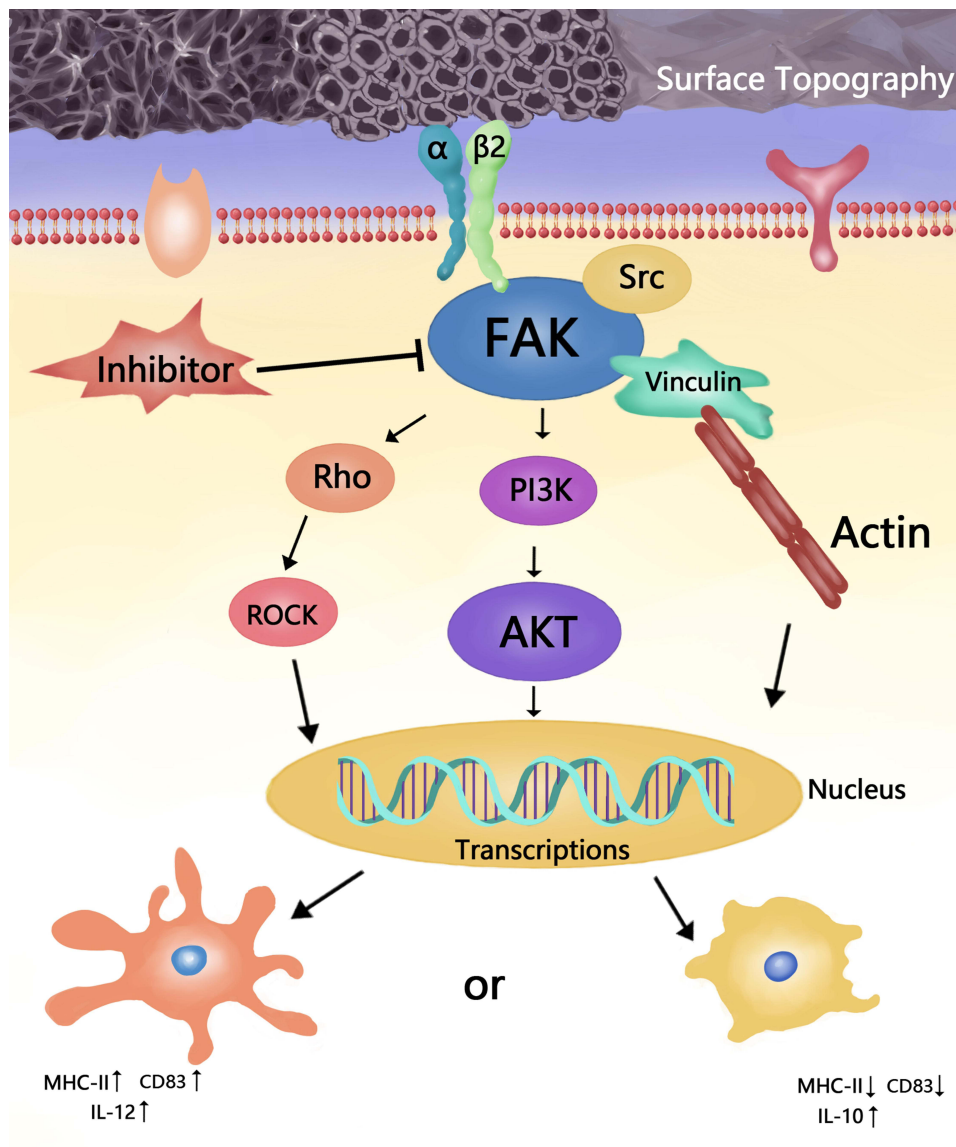
**Conclusion:** Compared to the SA surface with solely micro-scale topography, titanium surfaces with hybrid micro/nano-topographies reduced DC inflammatory response by influencing their adhesion states. This regulatory effect was accompanied by the modulation of  $\beta$ 2 integrin-FAK signal expression. The  $\beta$ 2 integrin-FAK-mediated adhesion plays a critical role in topography-induced DC activation, which represents a potential target for material–cell interaction regulation.

**Keywords:** micro/nanostructure, dendritic cell, osteoimmunology,  $\beta$ 2 integrin-FAK signal, surface modification

## Introduction

Dental implants are widely applied for the treatment of tooth loss with prominent therapeutic effects and high survival rates, as proven by numerous 10-year studies.<sup>1,2</sup> Titanium (Ti) and its alloys, with good biocompatibility and suitable mechanical properties, are the main biomedical materials used for the manufacturing of dental implants, and have been modified by various technologies for optimizing osseointegration properties.<sup>3,4</sup> Following implant positioning, numerous cells participate in implant–host interactions, and immune cells are the earliest to arrive and play critical regulatory roles during this process.<sup>5</sup> However, as foreign objects, titanium implants initiate immune reactions to different extents, which may potentially trigger unexpected inflammation and lead to fibrosis formation and implant rejection.<sup>6</sup> Considering that these side effects eventually

## Graphical Abstract



cause irreversible implant failure, avoiding or transforming risks related to immune response should be considered in biomaterial design.

After implantation, the innate and adaptive immune systems work together to build up a microenvironment around the implant and regulate the surrounding cell behavior.<sup>7</sup> Receptors on antigen-presenting cells (APCs) such as macrophages and dendritic cells will recognize the proteins adsorbed to the biomaterial surface and trigger phagocytosis.<sup>6,8</sup> As a key type of APCs,<sup>9</sup> dendritic cells (DCs) present antigens and pathogens and play an important role in inducing the primary immune response.<sup>10</sup> In the innate immune system, DCs secrete cytokines such as IFN- $\gamma$  and IL-12, which can activate or modulate other immune cells including eosinophils, macrophages, and natural killer cells.<sup>11</sup> In the adaptive immune system, DCs display peptide-major histocompatibility complexes that select rare antigen-specific T cells and initiate immune responses, generate cytotoxic T cells and activate B cells which perform their specific functions.<sup>12</sup> Upon contact with pathogens and inflammatory stimuli, DCs undergo activation and maturation to present antigens.<sup>10</sup> Although mature DCs take part in fighting

against tumors and pathogens, they readily give rise to an excessive inflammatory response and implant rejection. DCs can not only initiate immune responses but also exhibit tolerogenic properties in immature states.<sup>13</sup> Immature DCs, deficient in cell-surface costimulatory molecule expression, exhibit tolerogenic potential which may prolong allograft survival.<sup>14</sup> The tolerogenic properties of DCs are associated with T-cell anergy<sup>15</sup> and regulatory T-cell differentiation through the secretion of anti-inflammatory factors.<sup>16</sup> IL-10 secreted from tolerogenic DCs has also been shown to promote the differentiation of regulatory T cells, resulting in the suppression of inflammation and contributing to tissue healing.<sup>17,18</sup> Although the exact effects of DCs on biomaterial–host interactions have not been thoroughly investigated, the reduced activation of DCs has been suggested to dampen the inflammatory responses against implants, and thus guarantee and facilitate successful implant integration.<sup>19</sup>

In clinical scenarios, implants with microscale surface topography are commonly used due to their good performance in inducing osteoblast differentiation and obtaining initial tissue locking.<sup>20</sup> However, the hydrophobic microscale rough surfaces, with a low energy,<sup>21</sup> incline to facilitate the maturation and activation of immune members, including DCs, and induce an unfavorable immune condition that delays osteogenesis or threatens osseointegration.<sup>7,22,23</sup> Modification, such as endowing titanium with a hydrophilic surface, has been proven to alter immune cell functions, thereby accelerating the osseointegration process.<sup>24–26</sup> For this reason, nanoscale topography has been designed on the titanium surface for strengthening the regulatory effect on immune cell functions.<sup>24,27</sup> To endow the implants with combined advantages of both the microscale and nanoscale topography, nanoscale superstructure has been established onto a microscale basement to form a hybrid surface. Micro/nanostructures display biomimetic topography with high surface area and high porosity so that they imitate the extracellular matrix architecture of the host bone tissue and enhance the attachment of osteogenesis-related cells.<sup>28</sup> Such hierarchical micro/nano-topography on the biomaterial surface exhibited mixed features, resulting in improved immunomodulatory and osseointegration abilities compared with the microscale topography alone, as indicated by several studies concerning osteogenesis and the immune response on titanium alloy surfaces.<sup>29–31</sup> However, it is not clear whether nanomodification can modulate the activation of DCs or could maintain its immunotolerogenic state to ensure the successful host–biomaterial integration.

Implant surfaces have been designed to suppress the local inflammatory response and avoid excessive immune reactions.<sup>32</sup> After biomaterial positioning, infiltrated cells perceive and respond to extracellular substrate through various surface sensors including integrins, followed by cytoskeletal network remodeling, focal adhesions formation and the adjustments of cell shape, motility and function.<sup>33,34</sup> Based on the mechanical signal connection between cell membrane and nucleus, the extracellular stimuli of topography were transmitted into the cell to propagate downstream signals, like PI3K/AKT, RHOA/ROCK<sup>35,36</sup> and trigger corresponding immune responses. Integrins not only mediate cell–matrix adhesion but also control the cell sensing of geometry and rigidity of the extracellular environment.<sup>37</sup> Therefore, integrins have been demonstrated to play unique roles in the regulation of cell–topography interactions.  $\beta 2$  integrin (ITGB2) is expressed in most myeloid cells, including DC subsets, and participates in basic physiological and immune functions.<sup>38,39</sup>  $\beta 2$  integrin has regulatory functions in immune cell migration and adhesion<sup>40</sup> and is required for mediating DC adhesion as well as biomaterial-induced immune activation.<sup>41,42</sup> The blockage of  $\beta 2$  integrin can inhibit the adhesion of DCs and lower the extent of DC activation on polystyrene and poly(lactic-co-glycolic) acid films.<sup>41</sup> Integrin clustering induces the concentration and activation of a cytoplasmic tyrosine kinase, FAK.<sup>43</sup> As a critical downstream member of integrin as well as an effector in controlling cell adhesion and migration, FAK mediates signal transduction and participates in integrin-mediated cell functional adjustments.<sup>44,45</sup> Although  $\beta 2$  integrin has a close relationship with DC activation, whether the titanium surface affects DC activation through  $\beta 2$  integrin/FAK signal pathway remains unclear.

Therefore, we fabricated two micro/nano-hybrid topographies based on micro-level rough surfaces and employed the sand-blasted and acid-etched (SA) surface as a control, so as to investigate the potential role of micro/nanostructured topography in modulating DC activation and further elucidate the mechanism by which topography induced immune responses through the exploration of the  $\beta 2$  integrin/FAK signal pathway during this process.

## Materials and Methods

### Preparation and Characterization of Titanium Specimens

Titanium disks (thickness=1mm, diameter=21 mm or 10 mm) or titanium screws (diameter = 2.2 mm, length = 4 mm) were fabricated from commercially pure grade 4 titanium (Zhengfengyuan and Anchi, PR China). The disks were blasted with 250- $\mu$ m corundum particles and washed with 2 wt% HF to form the primary micro-scale basements. For SA surface preparation, the specimens were further immersed in the mixture of 98% H<sub>2</sub>SO<sub>4</sub> and 36.5% HCl solution (H<sub>2</sub>O/HCl/H<sub>2</sub>SO<sub>4</sub>, 2:4:3, v:v) at 90°C for 20 min to create a microscale topography. To fabricate surfaces with micro/nano structures, two kinds of specimens were prepared. For the sand-blasted, acid-etched and anodized (SAN) surface preparation, titanium specimens and platinum plates were connected to the anode and cathode of a DC constant power supply (Kwangduck FA, Korea), respectively. The specimens were treated at 20 V for 40 min in an electrolyte containing 0.5 wt % HF. For the sand-blasted, acid-etched and alkali-heated (SAA) group, titanium specimens were immersed in 5 M NaOH aqueous solution maintained at 80°C for 8 h. All specimens were washed with distilled water and sterilized in an autoclave before use. Surface composition and topography were characterized by X-ray energy-dispersive spectrometry (EDS) and field-emission scanning electron microscopy (FE-SEM; Hitachi S-4800, Japan). Surface roughness was analyzed using a contact profilometer (SJ-210, Japan), while hydrophilicity was analyzed using an OCA20 drop shape analysis system (DSA100, Germany).

### Animal Experiment

Twelve Sprague–Dawley rats (male, 300 g) were purchased from the Animal Experiment Center of Sun Yat-sen University. All animal experiment procedures were carried out in accordance with the methods approved by the Institutional Animal Care and Use Committee of Sun Yat-sen University (Application NO.2021001341). The welfare and treatment of the laboratory animals were carried out following the “Animal management regulations of China” and “Guangdong experimental animal management regulations”, published by State Scientific and Technological Commission of The People’s Republic of China and People’s Government of Guangdong Province, respectively.

The rats were randomly divided into experiments of two time points, and the rat femurs in each time point were randomly assigned into the SA, SAN and SAA groups. Rats were anaesthetized with 2% sodium pentobarbital (Sigma, USA). Subsequently, a 1 cm incision was made on the medial side of the knee joint, and the muscles were separated to expose the distal femur. On the inner side, 4-mm-deep holes were prepared using a 2-mm implant drill with sufficient saline cooling. Titanium specimen screws were positioned into the holes, and the surgical layers were successively sutured.

### Immunohistochemistry (IHC) Analysis and Histological Evaluation

IHC staining and histological evaluation were performed to evaluate the immune response after implant placement in vivo. For IHC staining, six rats were sacrificed at 7 days after surgery. The femurs with titanium screws were excised and kept in 10% neutral formalin for further evaluation. The femurs were decalcified in 10% EDTA (Sigma-Aldrich) for 45 days. The solution was replaced every 3 days followed by dehydration in a graded ethanol series (80–100%). The sample was then embedded in paraffin to prepare 5- $\mu$ m-thick thin sections utilizing a modified interlocked diamond saw (Leica Microtome, Wetzlar, Germany). For immunohistochemistry analysis, the sections were blocked with 5% BSA and incubated with anti-rat CD83 (1:100, #AF5233, Affinity, China) immunohistochemistry primary antibodies. The sections were then sequentially staining with undiluted horseradish peroxidase (HRP)-conjugated secondary antibody, diaminobenzidine (DAB) substrate, and hematoxylin. The stained samples were visualized using a digital scanner (Leica Aperio AT2, Germany), and the IOD (integrated optical density) of CD83-positive cells was quantified by Image Pro Plus software. For histological evaluation, the sections were stained with hematoxylin and eosin (H&E) to evaluate the inflammatory infiltration extent.

### Dendritic Cell Culture

The murine myeloid-derived immature dendritic cell line DC2.4 (Fuheng, China) was used in this study. DCs were cultured in RPMI 1640 medium with 10% fetal bovine serum (FBS) and maintained in 5% CO<sub>2</sub> and 95% air in

a humidified incubator at 37°C. The DCs were subcultured when they reached 80% confluence. In subsequent assays, unless specified otherwise, cells were subcultured on different titanium disks in 12-well plates with an initial density of  $2 \times 10^5$  cells per well.

## Cell Proliferation Assays

Direct cell counting assay and Cell Counting Kit-8 (CCK-8) analysis were used to detect cell proliferation. DCs were seeded in 48-well plates containing titanium specimens at a density of  $2 \times 10^4$  cells per well and cultured for 1, 2, or 3 days. For cell counting assay, cells were collected to form a single-cell suspension, followed by counting with an automatic cell counter (Nexcelom, USA). For CCK-8 analysis, complete medium containing 10% CCK-8 solution (Dojindo, Japan) was added and cells were incubated for 1.5 h. The medium was then collected, and the absorbance was measured at 450 nm using a multiskan ascent microplate reader (Tecan, Sunrise, Zurich, Switzerland).

## Flow Cytometry Analysis for DCs Apoptosis and Surface Marker

Flow cytometry analysis was performed for DCs apoptosis and maturation-related surface marker detection. After 24 h of culturing on titanium surfaces, DCs were collected by non-EDTA trypsin and washed twice with phosphate buffered saline (PBS). An Annexin V-fluorescein isothiocyanate apoptosis detection kit (Dojindo) was used for apoptosis detection. Cells in each group were resuspended with 100  $\mu$ L of binding buffer at a density of  $10^6$  cells/mL. Subsequently, the cells were incubated with Annexin V-FITC and propidium iodide (PI) for 15 min in the dark. Data were acquired with a flow cytometer (CytoFlex, Beckman, USA) and analyzed using CytExpert (Beckman). The apoptosis rates were calculated. For surface marker detection, cells were resuspended in PBS containing 2% bovine serum albumin (BSA) and stained with APC-labeled CD80 primary antibody (eBioscience, USA) for 1 h. After washing twice, data were acquired and analyzed as above.

## Quantitative Reverse Transcription Polymerase Chain Reaction (qRT-PCR)

The maturation and inflammation-related genes expression of DCs was evaluated by qRT-PCR. After culturing for 4 h or 24 h on titanium surfaces, the RNA of the DCs was collected using an RNA Quick Purification Kit (Yishan, China). The cells were disrupted in lysis buffer followed by the addition of the same volume of ethanol. The samples were mixed vigorously, centrifuged at  $12,000 \times g$ , and rinsed with wash buffer. After being dissolved in elution buffer, 500 ng total RNA was reverse transcribed to cDNA using a reverse transcription kit (TaKaRa, Japan). qRT-PCR was performed using SYBR Premix EX Taq (TaKaRa) in an ABI PRISM 7300 qRT-PCR system. The target genes were *IL-1 $\beta$* , *MHC-II*, *CD83* and *IL-10*, while the housekeeping gene glyceraldehyde-3-phosphate dehydrogenase (GAPDH) was served as a reference. The related primer was shown in [Table S1](#). Calculation of fold change was determined by the  $2^{-\Delta\Delta C_t}$  method.

## Fluorescent Microscopy

Immunofluorescence staining was performed to detect the cytoskeleton and CD83 expression of DCs. DCs were seeded on tissue culture plates or on titanium disks in 48-well plates at a density of  $2 \times 10^4$  cells per well. For cytoskeleton staining, after culturing for 4 h or 24 h, the samples were fixed with 4% paraformaldehyde at room temperature for 15 min and then permeabilized with 0.1% Triton X-100 in PBS for 10 min. F-actin was stained with FITC-phalloidin (1:100, C1033, Beyotime, China) and focal adhesion (FA) was detected with anti-vinculin antibody (1:100, ab129002, Abcam, UK) conjugated with Cy3-labeled second antibody (1:200, AS007, Abclonal, China), following which the nuclei were visualized with 4',6-diamidino-2-phenylindole (DAPI, C1005, Beyotime, China). Fluorescence images were captured using a confocal fluorescence microscope (Zeiss LSM780, Switzerland) under the magnification of 40 $\times$ .

For CD83 immunofluorescence assay, after culturing for 24 h, cells were fixed with 4% paraformaldehyde for 15 min and washed three times with PBST (0.1% Tween 20 PBS) at room temperature. The samples were blocked with 2% BSA in PBST and then incubated with CD83 antibody (1:50, A4234, Abclonal, China) for 60 min, following which they were stained with Cy3-labeled second antibody (1:200, AS007, Abclonal, China) for 60 min. The nuclei were stained by DAPI (C1005, Beyotime, China). Fluorescence images were captured, and the relative quantitative immunofluorescence intensity was measured using ImageJ through calculating the gray value.

## Enzyme-Linked Immunosorbent Assay (ELISA)

ELISA was utilized to detect the typical secreted markers which reflected the DCs activation states. The DCs culture medium was collected after 1 day of culturing. The medium was centrifuged at  $12,000\times g$ , and the supernatant was collected and stored at  $-80^{\circ}\text{C}$  until further utilization. The cytokine concentrations of IL-12 and IL-10 in the supernatant were detected using ELISA kits (Cusbio, China) according to the manufacturer's instructions. The absorbance at 450 nm was read, and the standard curve was constructed to quantify the cytokine concentrations.

For in vivo IL-12 detection, six rats were sacrificed 3 days after surgery. Then, 1-mm-thick tissues surrounding the titanium screw were harvested carefully by a trephine and then stored in liquid nitrogen. 100mg of samples were homogenized with 1mL PBS on the ice and then centrifuged for 10 min at  $12,000\times g$  and  $4^{\circ}\text{C}$ . The supernatant was collected, and the cytokine concentration of IL-12 was detected as described above.

## Western Blot Analysis

Western blot assays were used for detecting the protein expression of related signal pathway. After culturing for 4 h or 24 h, the cells on SA, SAN and SAA groups were lysed by RIPA lysis buffer (Beyotime, China), and total protein was collected after centrifugation at  $12,000\times g$  for 15 min. The protein concentration was assessed using a bicinchoninic acid assay kit (Cwbio, China). Overall, 20  $\mu\text{g}$  of total protein was separated using sodium dodecyl sulphate–polyacrylamide gel electrophoresis and transferred onto a polyvinylidene fluoride (PVDF) membrane (Millipore, USA). After blocking with 5% nonfat milk for 1 h at room temperature, the PVDF membrane was incubated with the primary antibodies at  $4^{\circ}\text{C}$  overnight. The primary antibodies included ITGB2 (1:1000, 72607, CST, USA), FAK (1:2000, ab40794, Abcam, UK), p-FAK (1:1000, ab81298, Abcam, UK), AKT (1:10000, ab179463, Abcam, UK), and p-AKT (1:1000, ab192623, Abcam, UK) antibodies. GAPDH (1:2000, 5174T, CST, USA) was used as a control. After washing three times with TBST (TBS with Triton X-100), the membranes were incubated with goat anti-rabbit secondary antibodies for 1 h at room temperature. The protein bands were incubated with an enhanced chemiluminescence substrate kit (ThermoFisher, USA) and then visualized with a chemiluminescence imaging system (GeneGnome XRQ, Syngene, UK). ImageJ software was used to assess the relative band intensities.

## Effect of FAK Inhibitor on DCs' Behavior

To detect the role of FAK in DCs' behavior, the responses of DCs on different topographies after FAK inhibition were also tested. Besides the application of inhibitor, all the experiments' procedure were performed as mentioned above. Cells were seeded into 96 well plates with 10  $\mu\text{M}$ , 5  $\mu\text{M}$ , 1  $\mu\text{M}$ , 0.1  $\mu\text{M}$  or without TAE226, a specific FAK activation inhibitor, respectively. The proliferation activity of cells was detected by CCK-8 at 1, 2, and 3 days after culturing. To detect the effect of FAK inhibitor on CD80 expression of DCs, cells were cultured for 24 h with 1  $\mu\text{M}$  or without TAE226, respectively, and the data were detected by Flow cytometry analysis. For inflammatory-related genes expression, cells were cultured on titanium plates (SA, SAN and SAA) with complete medium containing 1 $\mu\text{M}$  TAE226. After 24 h of culture, RNA was collected and inflammation-related genes *IL-1 $\beta$* , *MHC-II*, *CD83* and *IL-10* were detected by qRT-PCR. Immunofluorescence staining were performed to detect the cell morphology and CD83 expression after the samples were cultured with 1 $\mu\text{M}$  TAE226 for 24 h. Regarding the detection of signaling pathway after FAK inhibition, samples were cultured with 1 $\mu\text{M}$  TAE226 for 24 h and the expression level of FAK, p-FAK, AKT, and p-AKT were detected with Western Blot.

## Statistical Analysis

Unless otherwise specified, data are reported as the mean  $\pm$  standard deviation (SD) for each group with at least three replicates. The data were analyzed by analysis of variance followed by Bonferroni's multiple comparison test with GraphPad Prism 8 software (San Diego, CA, USA). Statistical significance was indicated by  $p < 0.05$ .

## Results

### Surface Characterization

SEM analysis showed that in the SA group, the titanium surface had micro-scale topography with undulating, irregular gullies. After anodization, uniform nanotubes with diameters of approximately 100 nm presented on the titanium surface

in the SAN group. In the SAA group, the surface had a net-like morphology containing irregularly distributed pores of varying sizes, and the main structures of pores appeared as 100 nm in diameters (Figure 1A).

The hydrophilicity of each group was analyzed by contact angle measurement. Among the groups, the contact angle was largest in the SA surfaces ( $76.63^\circ \pm 4.62^\circ$ ). In comparison, the samples of SAN and SAA groups had higher hydrophilicity, with the contact angles of approximately  $1.43^\circ \pm 2.03^\circ$  and  $19.93^\circ \pm 8.49^\circ$ , respectively (Figure 1B and C).

The roughness tests showed that the SA group had higher roughness  $2.82 \pm 0.06$  (Sa) than the SAN and SAA groups, which yielded roughness values of  $2.28 \pm 0.02$  (Sa) and  $2.57 \pm 0.10$  (Sa), respectively (Table 1). The EDS results showed that the proportion of oxygen on the titanium surface increased after micro/nano-modification, while the proportion of titanium decreased accordingly (Figure S1).

## DCs' Viability and Morphology

Through cell counting assays and CCK-8 analysis, we found that DCs presented higher proliferation rate in the SAN group, compared with that of the SA or SAA groups at all time points, with the SA and SAA groups exhibiting similar proliferation level (Figure 2A).

For DCs' morphology detection, we stained the cytoskeletons of cells cultured on tissue culture plate or titanium samples for 4 h or 24 h. DCs showed a round morphology on tissue culture plate at 4 h and 24 h without the stimulation of materials (Figure S2). After 4 h, the cells in the SA, SAN and SAA groups showed similarly round morphologies, with

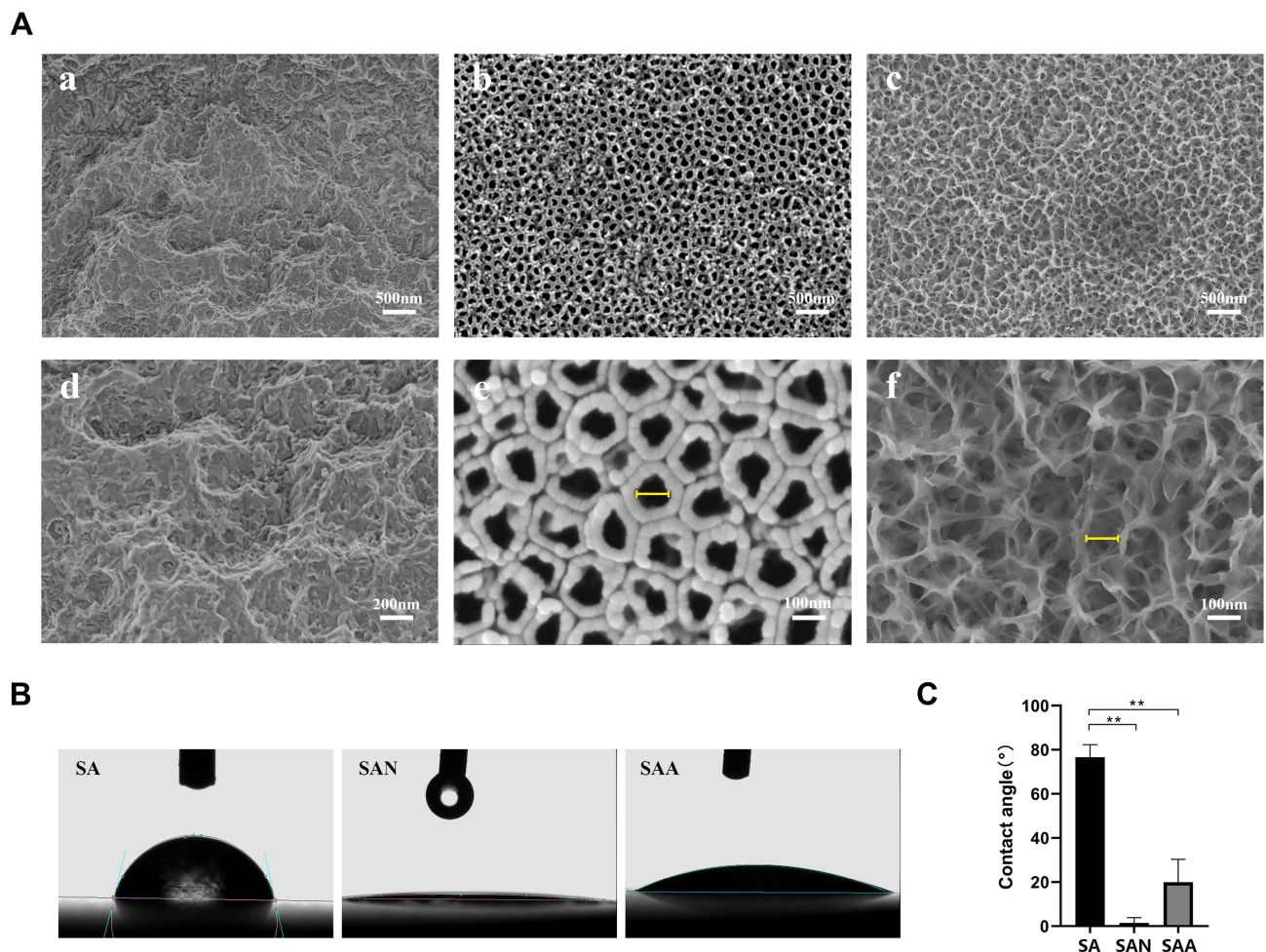


**Figure 1** Surface characterization of titanium samples. (A) SEM images showing the surface morphologies of the samples: SA (a, d) with consisting of micro-level irregular concavities and ridges without nanoscale structures, SAN (b, e) and SAA (c, f) showing microscale basements with specific surface nanostructures. Work distance: 4.4mm, Extra high tension: 5kV, Magnification:  $\times 5.0k-20.0k$ . The yellow bars are 100nm length. (B and C) The results of contact angle test on different titanium surfaces. Data represented as mean $\pm$ SD, n=3. \*\*P < 0.01 when compared to the SA group.

**Table 1** Roughness Measurements of Samples (n=3, Mean  $\pm$  SD)

Samples	Sa ( $\mu\text{m}$ )	Sq ( $\mu\text{m}$ )
SA	2.82 $\pm$ 0.06	3.57 $\pm$ 0.08
SAN	2.28 $\pm$ 0.02**	2.88 $\pm$ 0.03**
SAA	2.57 $\pm$ 0.10*	3.25 $\pm$ 0.17

**Notes:** Sa (arithmetic mean height); Sq (root mean square height). \*P < 0.05 and \*\*P < 0.01 when compared to the SA group.

several cells exhibiting slight spreading (Figure S3). After 24 h of attachment, the cells in the SA group showed star-like or irregular adhesion patterns with outstretched branches, while cells in the SAN and SAA groups retained rounder shapes without obvious branches (Figure 2B).

Flow cytometry showed that the DCs on different titanium surfaces had similar apoptosis rate, indicating that the micro- or micro/nanostructures of titanium surface had no obvious cytotoxic effect on the DCs' viabilities (Figure 2C and D).

### Expression of Genes Related to DC Activation

The expressions of genes related to DC activation were evaluated using qRT-PCR at 24 h after cell seeding on the titanium surfaces (Figure 3A). After 24 h culture, among the groups, the expressions of *CD83*, *MHC-II*, and *IL-1 $\beta$*  genes, which are related to DC maturation or inflammation states, were highest in the SA group. Lower gene expressions were found in the SAN and SAA groups, with SAN showing the lowest expressed level of *MHC-II* and *IL-1 $\beta$*  genes, and SAA showing the lowest expression level of *CD83* gene. The expression of anti-inflammation gene *IL-10* was lowest in the SA group and highest in the SAA group, which showed an opposite trend with those genes mentioned above. After 4 h culture, the expression of *CD83*, *MHC-II*, *IL-1 $\beta$*  and *IL-10* genes showed no significant differences among three groups (Figure S4).

### Flow Cytometry Detection of DC Surface Markers

Using flow cytometry, we detected the expressions of DC maturation markers CD80 at 24 h after the cells were seeded on the titanium surface (Figure 3B). At 24 h after seeding, the expressions of CD80 in the SA group were higher than those in the SAN and SAA groups with the rate of CD80-positive cells decreasing in the order of SA > SAN > SAA.

### Immunofluorescence of DCs' Marker

Immunofluorescence was utilized for DCs' surface marker CD83 detection (Figure 3C). The calculated results of staining pictures showed that the CD83 fluorescence intensity was highest in the SA group, while the difference in CD83 fluorescence intensity between the SAN and SAA groups was not significant (Figure 3D).

### ELISA Determination of Inflammatory-Related Cytokines

The expressions of IL-10 and IL-12 cytokines related to DC maturing status were detected by ELISA after culturing for 24 h (Figure 3E). The expression of IL-10 was significantly higher in SAN and SAA groups compared to the SA group and the expression of IL-10 was slightly higher in the SAN group than in the SAA group. The results demonstrated that the expression of IL-12 was obviously higher in SA group than SAA group, while the difference was not significant between SA and SAN groups.

### Detection of $\beta$ 2 Integrin-FAK-AKT Signals

At 4 h and 24 h after seeding the DCs on the titanium surface, we collected cell proteins to detect changes in the  $\beta$ 2 integrin-FAK-AKT signal pathway through Western blotting (Figure 4A–D). The expression of  $\beta$ 2 integrin was higher in the SA group than in the SAN and SAA groups, and the differences were significant at both 4 h and 24 h. Meanwhile,



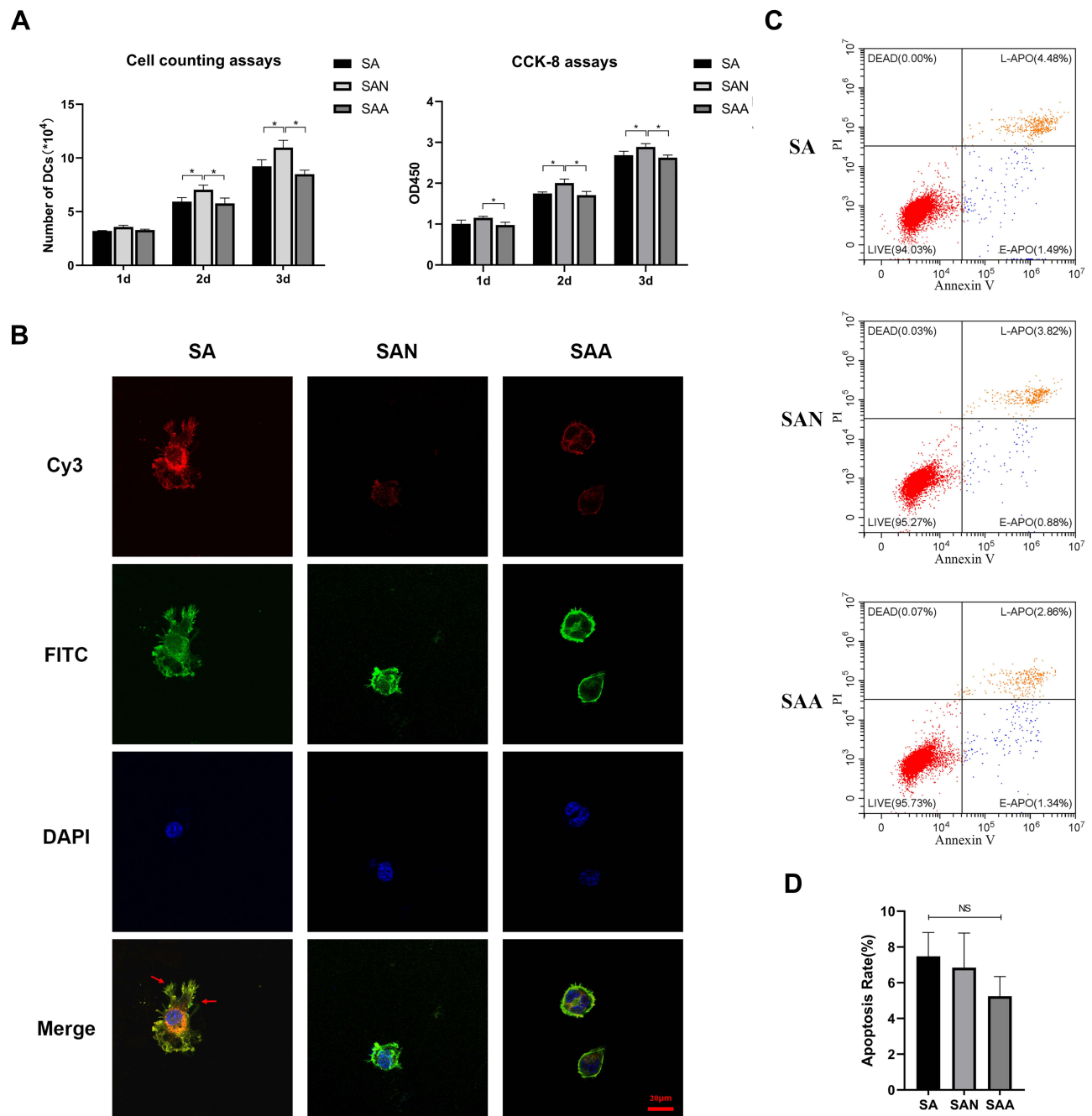


**Figure 2** Analysis of DC viability and morphology on different titanium surfaces. **(A)** Cell counting assay and CCK-8 detection of cell proliferative activity at 1, 2 and 3 days. **(B)** The fluorescent staining images of vinculin (Red), F-actin (Green) and nuclei (Blue) showing the DC morphologies on different titanium surfaces at 24 h. Arrows: branch-like protrusion of DCs. **(C)** Analysis of DC apoptosis at 24 h by flow cytometry and **(D)** the calculation of apoptosis rate (Early apoptosis and late apoptosis). Data represented as mean $\pm$ SD, n=3. \* $P < 0.05$  when compared to the SAN group.

**Abbreviation:** NS, not significant.

the SAA group expressed the lowest level of  $\beta 2$  integrin. The expressions of p-FAK and FAK, which had similar tendency to  $\beta 2$  integrin when compared with GAPDH, were simultaneously higher in the SA group than in the SAN and SAA groups with significant differences at both 4 h and 24 h. Regarding the downstream pathway, no significant differences in the expressions of p-AKT and AKT were observed among the three groups at 4 h. At 24 h, the expression of p-AKT and the phosphorylation ratio of p-AKT/AKT were significantly higher in SA group than in SAN and SAA groups.

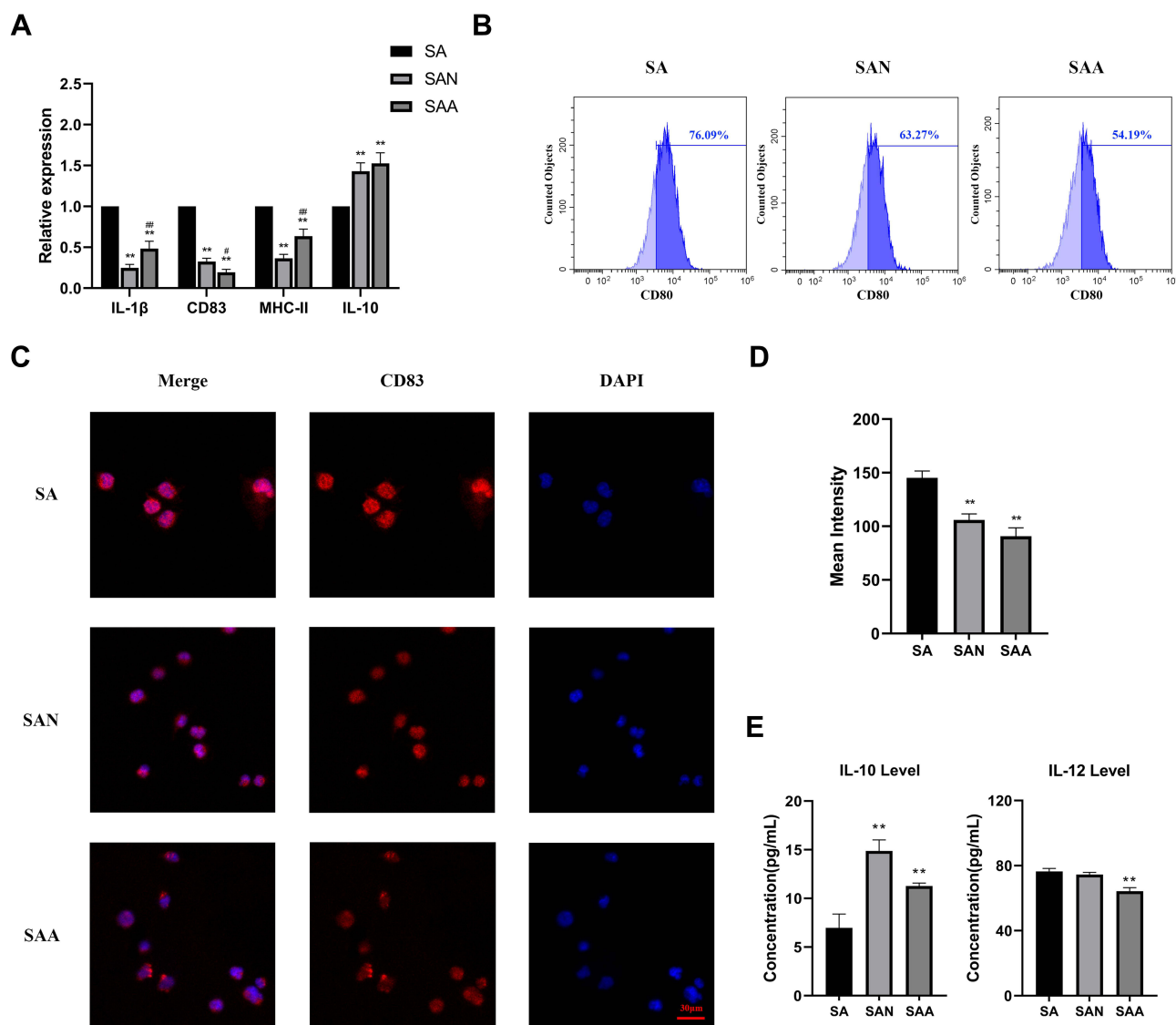


**Figure 3** DC immune responses on different titanium surfaces. (A) Relative gene expressions of activation markers IL-1 $\beta$ , CD83, MHC-II and IL-10 at 24 h. (B) Flow cytometry results showing the expressions of activation-related markers CD80 at 24 h. (C) Immunofluorescence staining images showing the CD83 expressions of DCs on different titanium surfaces at 24 h, (D) and the relative CD83 fluorescence intensities. (E) The detection of IL-10 and IL-12 secreted by DCs utilizing ELISA after 24 h culture. Data represented as mean $\pm$ SD, n=3. \*\**P* < 0.01 when compared to the SA group; #*P* < 0.05 and ##*P* < 0.01 when compared to the SAN group.

### In vivo Experiment

Seven days after implantation, H&E staining results showed a small amount of the inflammatory cell infiltrates in three groups (Figure 5A). We detected the expressions of CD83 via the immunohistochemical staining of the tissues surrounding the screw threads (Figure 5A). Significantly higher IOD value of CD83-positive-staining cells was measured in the SA group than in the SAN and SAA groups (Figure 5B).

Three days after implant placement, the samples were harvested for ELISA detection. We evaluated the expression of IL-12 in the tissues around the implants and found that among three groups, the IL-12 concentration was lowest in the SAA group, and highest in the SA group (Figure 5C).

### DCs Responses After FAK Inhibition

The proliferation activity of DCs decreased significantly cultured at relatively higher concentration of TAE226 (10  $\mu$ M and 5  $\mu$ M). When cultured with the inhibitors below 1  $\mu$ M of concentration, cells presented no significant difference in

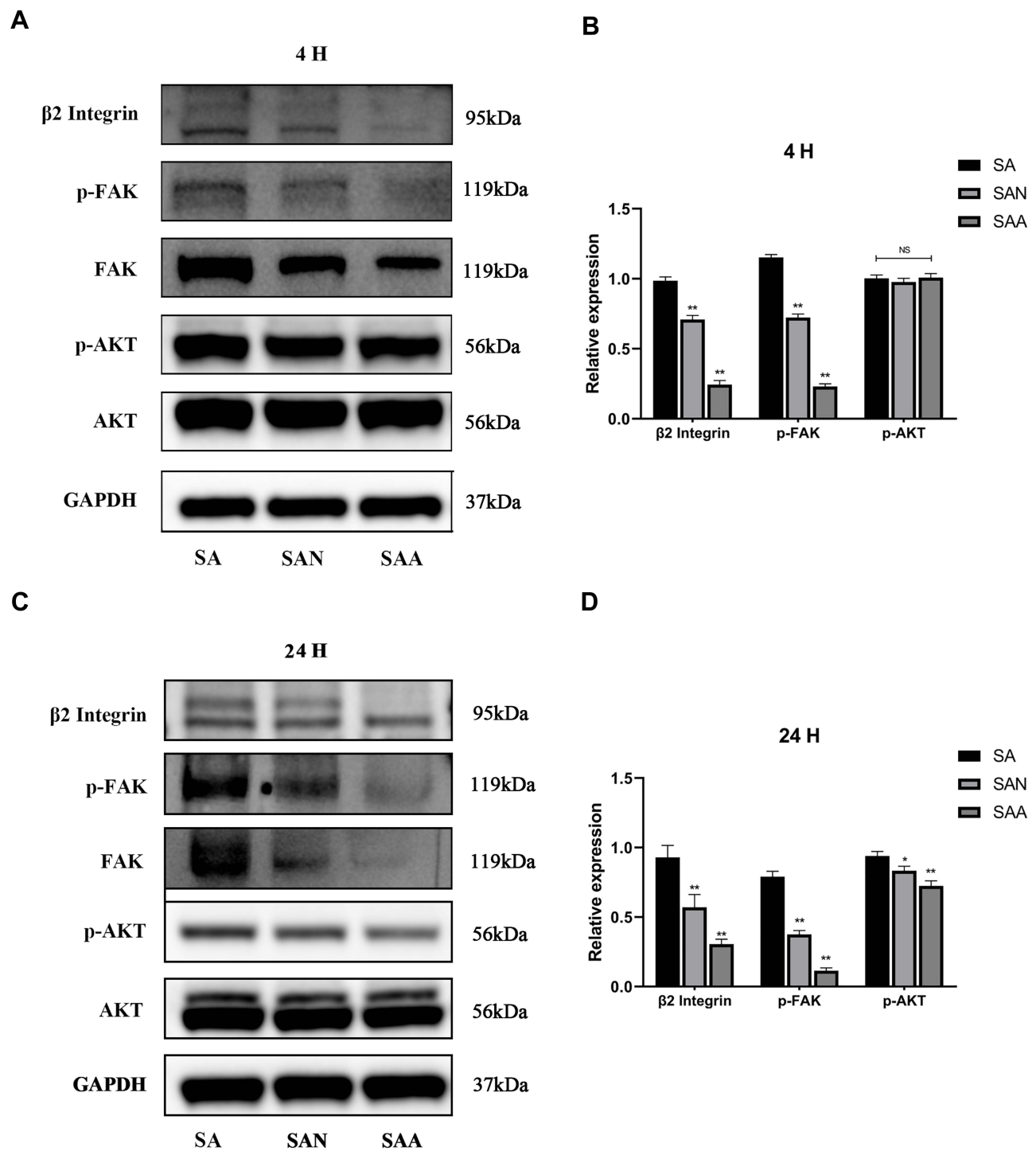


**Figure 4** Detection of DC adhesion and maturation-related signals. The protein bands of  $\beta 2$  integrin, p-FAK, FAK, p-AKT, and AKT and the relative expressions of p-FAK/GAPDH and p-AKT/AKT at 4 h (**A** and **B**) and 24 h (**C** and **D**). Data represented as mean $\pm$ SD, n=3. \* $P < 0.05$  and \*\* $P < 0.01$  when compared to the SA group. **Abbreviation:** NS, not significant.

cell proliferation ability compared with the control group within 2 days ([Figure S5](#)). The expression of CD80 after treated with 1 $\mu$ M of TAE226 was downregulated when compared with untreated group ([Figure S6](#)).

After cultured with 1 $\mu$ M TAE226 for 24 h, the expression of CD83, MHC-II and IL-1 $\beta$  in the SA group were significantly down-regulated, while their differences among three groups were also narrowed. IL-10 expression was up-

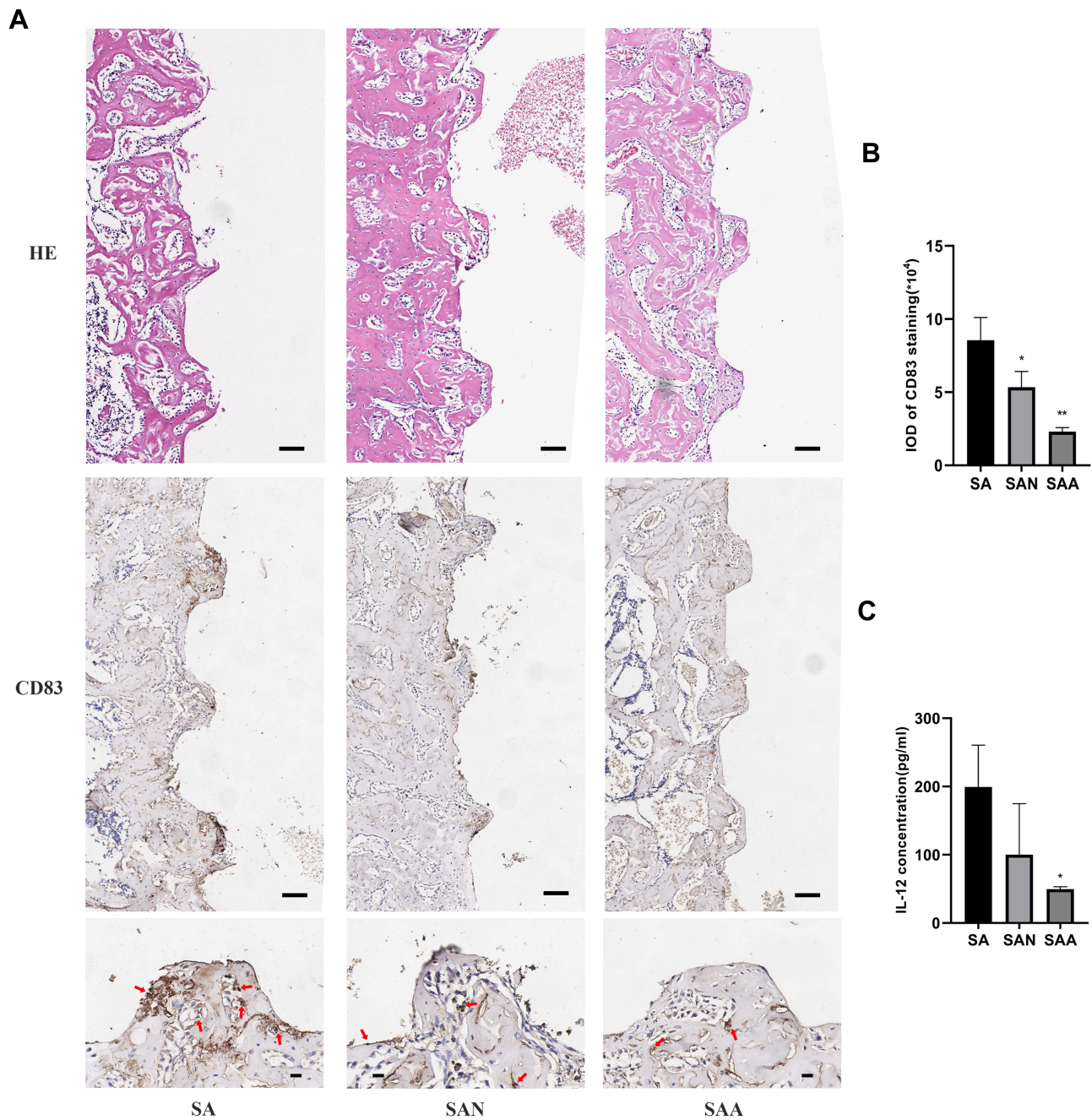


**Figure 5** In vivo evaluation DC immune responses around implants. **(A)** Hematoxylin and eosin (H&E) staining and representative immunohistochemical images of CD83 at the bone–implant interface at 7 days after implantation with the close-up images. **(B)** The IOD values of CD83-positive cells counted by ImagePro Plus in the region of interest. **(C)** Local IL-12 level within 1 mm around the implant site at 3 days after implantation based on ELISA. Arrows: CD83-positive cells. Scale bar = 100 μm. Data represented as mean±SD, n=4. \*P < 0.05 and \*\*P < 0.01 compared to the SA group.

regulated, without significance difference among three groups(Figure 6A). The relative expression of p-FAK decreased significantly with no significant differences among three groups. Although p-AKT expression was slightly higher in SA, no significant differences were counted among the three groups (Figure 6B). Cells exhibited round morphology with rarely stretched pseudopodia on all titanium surfaces (Figure 6C), and their differences in the fluorescence intensity of CD83 were not significant (Figure 6D).

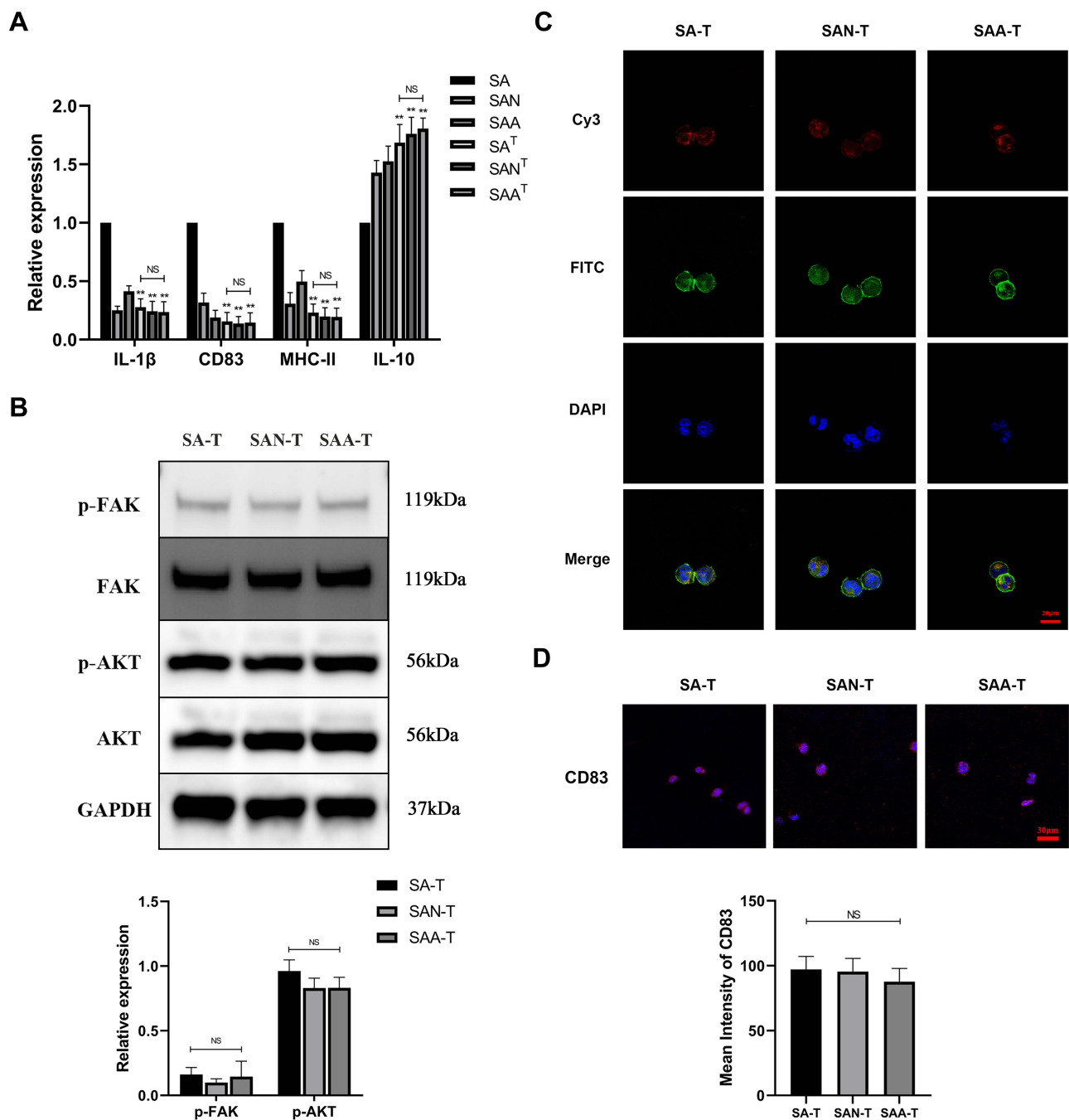


**Figure 6** The analysis of DC responses after FAK inhibition. **(A)** DC activation-related genes *IL-1 $\beta$* , *CD83*, *MHC-II* and *IL-10* expression on different titanium surfaces after 1 day culture with (SA-T, SAN-T, SAA-T) or without (SA, SAN, SAA) TAE226, respectively **(B)** The protein bands and relative expression of DC p-FAK/FAK and p-AKT/AKT signals by Western blotting assays after FAK inhibition. **(C)** The fluorescent staining images of vinculin (red), F-actin (green) and nuclei (blue) showing the DC morphologies and **(D)** CD83 staining on different titanium surfaces after FAK inhibition, and the relative fluorescence intensities of CD83 were calculated. Data represented as mean $\pm$ SD, n=3. \*\* $P < 0.01$  when compared to the SA group. **Abbreviation:** NS, not significant.

## Discussion

The response of immune cells has proven relevant to the success ratio of implant bone integration. After implantation, the unwanted immune cascade of defense cells is detrimental to wound healing and tissue integration.<sup>46,47</sup> Most immune cells, such as macrophages, DCs, and T cells, have bifunctional anti-inflammatory and proinflammatory properties.<sup>48–50</sup>

Therefore, transforming the immune cells into a favorable immune direction and reducing the unnecessary immune response by processing the implant materials are important considerations in immune-informed biomaterial development.<sup>47,51</sup> An ideal biomaterial elicits an appropriate immune cell response that guarantees tissue restoration while also promoting osteogenesis behaviors of tissue repair cells.

Modification of biomaterial surfaces is a feasible strategy for altering unfavorable immune responses. Tailoring the biomimetic titanium surface on Ti material has attracted much attention for its advantages in biocompatibility and osseointegration.<sup>52</sup> In natural condition, the structure of bone tissue varies at the micro- and macro-size scales.<sup>53</sup> Cortical bone reveals different scale of porous structures with the cancellous bone.<sup>54</sup> Recently, investigations in biomimetic surface designs have shifted towards hierarchical micro/nanostructures which mimic the natural bone matrix and promoting the implant–host immune reactions. Previous researches indicated that the nanostructures simulated the size and the arrangement of nanoscale collagen fibers of the bone tissue,<sup>55</sup> while the hierarchical micro/nanostructures better mimicked the natural extracellular matrix (ECM) of bone, which was mainly composed of 50–500 nm collagen fibers.<sup>56</sup> Bai et al unraveled that micro/nanostructure in such ranges was biomimetic which warrant the amelioration of inflammation and acceleration of osseointegration.<sup>28</sup> Therefore, tailoring the biomimetic titanium surface on Ti material has attracted much attention for its advantages in biocompatibility and osseointegration. In this study, we established the nano-scale supra-structure onto micro-scale basement which was constructed by sandblasted and acid etching, in order to mimic the structure of clots with 3D fiber networks in the early healing stage, which not only enables a robust osteoimmunomodulation effect but also significantly enhances osseointegration.<sup>57,58</sup> Our hierarchical micro/nano-topographies had similar microscopic structures that successfully obtained preferable immune responses, which proved that biomimetic designs had a considerable prospect in clinical application.

Surfaces with micro/nano-topographies possess the advantages of osteogenic differentiation and initial stabilization inherited from the microscale basement,<sup>59,60</sup> along with the ability to regulate cell proliferation and immune response originating from the nanoscale structure.<sup>61,62</sup> Anodic oxidation has been widely used to build uniform nanotubes,<sup>62</sup> while alkali/heat treatment is commonly used to form irregular nanonets.<sup>63</sup> The effects of nanotopography on DC behaviors have neither been investigated nor have the effects on DC behaviors been compared between microtopographies and nanotopographies. Thus, we established two different nanotopographies on microscale substrates and compared their effects on DCs with SA surfaces. Both the main structures of nanotubes in SAN and nanonets in SAA were designed with similar sizes for comparison and were proven to have good biocompatibility and osteogenesis behaviors in earlier studies.<sup>64,65</sup> Surface characterization showed that both the SAN and SAA groups had slightly lower roughness and significantly higher hydrophilicity than the SA group, which was due to the nanostructure exhibiting a less rugged surface than the microstructure.<sup>66</sup> We speculated that the nanostructure with higher surface areas enables the hydrophilicity reactions to take place, while the anatase phase formed on titanium surface also contributes to the hydrophilic characteristics.<sup>67</sup> Previous research proposed that proper roughness was beneficial for modulating immune responses,<sup>68</sup> and the micro/nanostructured surfaces in this study manifested medium roughness, which had the potential to trigger a weaker proinflammatory response of macrophages.<sup>69</sup> However, the dynamic relationships between roughness and DC behaviors are still unclear. The SAN and SAA surfaces here share similar characteristics with the modSLA surface with hydrophilic treatment, which was shown to benefit implant osseointegration by promoting a tolerant DC phenotype,<sup>70</sup> indicating that hydrophilicity also plays a critical role in determining DC responses. Therefore, considering the changes in hydrophilicity and roughness after surface modifications, we will further explore whether modified topography modulates DC behaviors via changed surface characteristics, such as roughness and hydrophilicity, or the topography factor itself.

Behaviors of DCs cultured on the materials can be altered by surface modification. The proliferation of cells was significantly improved in the SAN group compared to the SAA and SA groups while they all had similar apoptosis rate, indicating that differences in nanostructure pattern also influences cellular basic physiological behaviors. However, cell proliferation was determined by a wide variety of factors, which did not reach a unified conclusion.<sup>71–73</sup> We hypothesize that the orderly arranged nanotubes that accelerate protein adsorption enhance cellular proliferative activity.<sup>74</sup> The expression of surface markers or inflammatory factors in DCs represents their immune status. In the present study, after culturing for 24 h, qRT–PCR analysis showed that the expression levels of genes related to DC maturation and

inflammation were significantly higher in the SA group than in the SAN and SAA groups, while the SA group showed a relatively lower anti-inflammatory gene expression. Flow cytometry and immunofluorescence analyses confirmed that the expression levels of DC maturation markers CD80 and CD83 were lower in the SAN and SAA groups than in the control. These findings demonstrated that micro/nanostructures inhibited DC activation and reduced the expression of inflammatory-related factors, in accordance with findings revealing that micro/nanostructures inhibit the proinflammatory response of other typical immune cells, such as macrophages.<sup>28</sup> Activated DCs secrete IL-12 and promote the Th1/Th17 inflammatory response, whereas tolerogenic DCs express the anti-inflammatory cytokine IL-10, which prevents tissue damage.<sup>17,75,76</sup> The *in vitro* ELISA results demonstrated that the expression of IL-12 was slightly higher in the SA group than in the other two groups and the significant difference only existed between the SA and SAA groups, while the level of IL-10 was significantly higher in the SAN and SAA groups than in the SA group. Considering the higher cellular proliferative activity in SAN compared to SA, as demonstrated by cell counting and CCK-8 analysis, IL-12 secretion would be significantly increased in SA compared to the other two groups if normalizing for cellular proliferative activity. Therefore, we concluded that DC activation and the release of related factors can be altered by modifying the microscale surface with nanostructures. Slight differences were found between the nanotube and nanonet structures. Although the nanotubes in the SAN group induced more favorable DC proliferation activity, the DCs on the nanonets in the SAA group expressed lower levels of maturation-related genes, surface markers, and proinflammatory cytokines. These divergences between DC activation and behaviors on different surfaces suggest that the local environment also affects DCs in addition to their activation status. The slight differences between micro/nano-topographies in affecting DC behaviors may be due to changes in multiple aspects of physical properties, such as hardness, surface charge and superficial structure, which influence cell surface integrin ligand arrangement, nutrient uptake, and multiple physiological activities.<sup>77-79</sup> The effects of specific local environmental factors on DC behaviors thus require further study.

DCs adhesion condition, influenced by surface morphology of titanium through  $\beta 2$  Integrin-FAK signals, can determine DCs' immune response. Possible processes of titanium micro/nanostructured topography that influence dendritic cells via  $\beta 2$  Integrin-FAK signals are summarized in the graphical abstract. The surface topography affects the cell behaviors most directly via cell sensing and adhesion.<sup>80</sup> Numerous studies have focused on adhesion-guided surface modification to improve the cell response from the perspective of immune regulation.<sup>47,70,81</sup> We evaluated the attachment process by F-actin and vinculin staining, revealing the distinct adhesion morphologies among the experimental groups. Although cells in the three groups adhered with almost the same morphologies at 4 h, the DC adhesion showed more bifurcations and a wider spreading extent in the SA group than in the SAN and SAA groups at 24 h. These differences in attachment behavior were associated with the activated states of the DCs to some extent.<sup>82</sup> Previous studies supported that the shaping of cell adhesion determined their immune responses, indicating the feasibility of immune status regulation by modulating cell adhesion conditions.<sup>83</sup> From this perspective, we investigated the changes in  $\beta 2$  integrin-FAK signal, which dominantly participated in cell environmental perception and adhesion. In the early stage of adhesion, the DCs showed no differences in activation or cytokine secretion among the groups at 4 h, while the expression of  $\beta 2$  integrins was significantly higher in the SA group than in the other two groups in the late stage of adhesion (24 h). Both p-FAK and FAK were also highly expressed at 24 h in the SA group, which might be due to FAK's role as one of the main components of adhesion plaques, accompanied by FAK-related signal activation, as a result the relative expression of p-FAK/GAPDH was calculated in representing the overall FAK level. Similar trends were also observed at the 4 h time point, indicating that the SA morphology stimulated the expression of DC integrins in the early stage of cell attachment, thereby inducing rapid FAK activation and pseudopodia formation. Moreover, the spreading of DCs shared the same trend with FAK expression, which was also confirmed by Serrels<sup>84</sup> that cell adhesion was significantly related to FAK.  $\beta 2$  Integrin-FAK activation induces DC activation via downstream pathways, among which the PI3K/AKT signal pathway is important for regulating complicated cell physiological activities.<sup>85</sup> PI3K/AKT was also proven to positively regulate DC maturation along with their functional status.<sup>86</sup> In the present study, the activated AKT of different groups showed the same trend as FAK expression at 24 h. However, the differences in activated AKT between groups were not significant at 4 h, consistent with the DC activation state. Therefore, we concluded that the activation of PI3K/AKT was closely related to DC activation and PI3K/AKT signal was activated by integrin-FAK along with cell adhesion processes, leading to completely different DC performances between 4 h and 24

h. We demonstrated the regulatory effect of the  $\beta 2$  integrin-FAK-AKT signal chains on DC activation on titanium surfaces. FAK signal not only controls AKT but also regulates other downstream effectors, such as MAPK and the Rho-GTPase family,<sup>87,88</sup> which play specific roles in modulating DC immune responses. We found that AKT expression was not significantly suppressed after FAK inhibition, which may be due to other signals upstream of AKT remaining normally expressed. The inhibited FAK influenced DC adhesion and suppressed the topography-mediated DC activation differences, which inspired us to conclude that adhesion-related signals control topography-cell interactions and that regulating FAK-related signals affected the influence of the environment on cell adhesion and function. It was noteworthy that after FAK inhibition, the expression of anti-inflammatory related gene IL-10 was elevated. We speculated that FAK inhibitor significantly reduced the DCs activation on titanium surface and enabled DCs to maintain a relatively high expression of IL-10. Our results supported that the inhibited FAK alleviated the impact of titanium on DCs and further reduced the activation level. For this reason, we believe that directly regulating the upstream integrin-FAK pathway by adjusting the topography of the implant surface is a more effective way to regulate the cell response than changing downstream signals via biological methods. However, integrins and FAK perform complex roles in DC activation as well as other fundamental activities, while inhibition of FAK also influences the proliferation and viability of DCs. Therefore, the specific effects of  $\beta 2$  integrin-FAK signal on the biological behaviors of DCs, the precise utilization of adhesion signals in controlling the DC immune response as well as the involvement of other integrin families in this process require further verification.

Through *in vivo* studies, we investigated the local expression of markers and cytokines related to DC activation and found that the *in vivo* results had similar trends to the *in vitro* results. Although CD83 has been proven to be a typical marker of mature DCs while the inflammatory cytokine IL-12 is the major bioactive product from DCs in immune communication,<sup>89,90</sup> such indices also exist in some other immune cells, such as macrophages and B lymphocytes.<sup>91,92</sup> Watford<sup>93</sup> revealed that other immune members, especially macrophages, also secreted a certain amount of IL-12 *in vitro*, while DCs are the major source of IL-12 *in vivo*. Therefore, our *in vivo* results revealed the overall immune cell functional status, which represented DCs around implants to a great extent. The present study was limited to the behaviors of DCs, while the interaction of DCs with other immune cells was not investigated because of the complex immune networks *in vivo*. We believe that the regulatory effects of cells can also influence DCs, while the cell-cell interactions call for further exploration. The *in vivo* behaviors of micro/nanostructures on osseointegration were better than those of microstructures,<sup>30,94</sup> but the direct clues of DC behaviors and osseointegration have not been thoroughly explored. Thus, future work will focus on exploring the specific roles of DCs in osseointegration and the contributions of different DC phenotypes to osseointegration.

## Conclusion

Titanium surfaces with hybrid micro/nano-topographies reduced dendritic cell inflammatory response by influencing their adhesion states compared to the SA surface with solely micro-scale topography. This regulatory effect was accompanied by modulating expression of  $\beta 2$  integrin-FAK, an adhesion-related signal chain which was proven to have a close relationship with DC activation. There also existed slight differences of DC activation on two typical nanostructures, among which nano-net exhibited more immature DCs' phenotype as well as less inflammatory responses. The changes in the adhesion-related  $\beta 2$  integrin-FAK signaling pathway were initiated in the early stage of adhesion, while the changes in downstream signals and DCs' activation appeared in the late stage of adhesion. The inhibition of FAK signal could not only reduce the mature level of DCs but also narrow the differences among various topography-induced DCs' activation activities, which represented an effective target for biomaterial topography design and cell interaction regulation.

## Acknowledgments

The authors thank all of the research staff members at the Department of Oral Implantology, Guanghua School of Stomatology, Sun Yat-sen University. The work was supported by the Guangdong Provincial Science and Technology Major Project (No. 2017B090912004).



## Disclosure

The authors declare that the research was conducted in the absence of any commercial or financial relationships that could be construed as a potential conflict of interest. The authors report no conflicts of interest in this work.

## References

1. Monje A, Alcoforado G, Padiál-Molina M, Suarez F, Lin GH, Wang HL. Generalized aggressive periodontitis as a risk factor for dental implant failure: a systematic review and meta-analysis. *J Periodontol*. 2014;85(10):1398–1407. doi:10.1902/jop.2014.140135
2. Buser D, Sennerby L, De Bruyn H. Modern implant dentistry based on osseointegration: 50 years of progress, current trends and open questions. *Periodontol 2000*. 2017;73(1):7–21. doi:10.1111/prd.12185
3. Costa RC, Nagay BE, Bertolini M, et al. Fitting pieces into the puzzle: the impact of titanium-based dental implant surface modifications on bacterial accumulation and polymicrobial infections. *Adv Colloid Interface Sci*. 2021;298:102551. doi:10.1016/j.cis.2021.102551
4. Attarilar S, Salehi MT, Al-Fadhlah KJ, Djavanroodi F, Mozafari M. Functionally graded titanium implants: characteristic enhancement induced by combined severe plastic deformation. *PLoS One*. 2019;14(8):e0221491. doi:10.1371/journal.pone.0221491
5. Hotchkiss KM, Clark NM, Olivares-Navarrete R. Macrophage response to hydrophilic biomaterials regulates MSC recruitment and T-helper cell populations. *Biomaterials*. 2018;182:202–215. doi:10.1016/j.biomaterials.2018.08.029
6. Jones KS. Effects of biomaterial-induced inflammation on fibrosis and rejection. *Semin Immunol*. 2008;20(2):130–136. doi:10.1016/j.smim.2007.11.005
7. Baseri M, Radmand F, Hamed R, Yousefi M, Kafil HS. Immunological aspects of dental implant rejection. *Biomed Res Int*. 2020;2020:7279509. doi:10.1155/2020/7279509
8. Thiele L, Diederichs JE, Reszka R, Merkle HP, Walter E. Competitive adsorption of serum proteins at microparticles affects phagocytosis by dendritic cells. *Biomaterials*. 2003;24(8):1409–1418. doi:10.1016/S0142-9612(02)00525-2
9. Esterházy D, Loschko J, London M, Jove V, Oliveira TY, Mucida D. Classical dendritic cells are required for dietary antigen-mediated induction of peripheral T(reg) cells and tolerance. *Nat Immunol*. 2016;17(5):545–555. doi:10.1038/ni.3408
10. Théry C, Amigorena S. The cell biology of antigen presentation in dendritic cells. *Curr Opin Immunol*. 2001;13(1):45–51. doi:10.1016/S0952-7915(00)00180-1
11. Banchereau J, Briere F, Caux C, et al. Immunobiology of dendritic cells. *Annu Rev Immunol*. 2000;18:767–811. doi:10.1146/annurev.immunol.18.1.767
12. Constantino J, Gomes C, Falcão A, Neves BM, Cruz MT. Dendritic cell-based immunotherapy: a basic review and recent advances. *Immunol Res*. 2017;65(4):798–810. doi:10.1007/s12026-017-8931-1
13. Dhodapkar MV, Steinman RM, Krasovsky J, Munz C, Bhardwaj N. Antigen-specific inhibition of effector T cell function in humans after injection of immature dendritic cells. *J Exp Med*. 2001;193(2):233–238. doi:10.1084/jem.193.2.233
14. Lu L, Lee WC, Takayama T, et al. Genetic engineering of dendritic cells to express immunosuppressive molecules (viral IL-10, TGF-beta, and CTLA4Ig). *J Leukoc Biol*. 1999;66(2):293–296. doi:10.1002/jlb.66.2.293
15. Macián F, Im SH, García-Cózar FJ, Rao A. T-cell anergy. *Curr Opin Immunol*. 2004;16(2):209–216. doi:10.1016/j.coi.2004.01.013
16. Huang H, Dawicki W, Zhang X, Town J, Gordon JR. Tolerogenic dendritic cells induce CD4+CD25hiFoxp3+ regulatory T cell differentiation from CD4+CD25-/-loFoxp3- effector T cells. *J Immunol*. 2010;185(9):5003–5010. doi:10.4049/jimmunol.0903446
17. Schülke S. Induction of interleukin-10 producing dendritic cells as a tool to suppress allergen-specific T helper 2 responses. *Front Immunol*. 2018;9:455. doi:10.3389/fimmu.2018.00455
18. Kumar V. T cells and their immunometabolism: a novel way to understanding sepsis immunopathogenesis and future therapeutics. *Eur J Cell Biol*. 2018;97(6):379–392. doi:10.1016/j.ejcb.2018.05.001
19. Eslami-Kaliji F, Sarafbidabad M, Rajadas J, Mohammadi MR. Dendritic cells as targets for biomaterial-based immunomodulation. *ACS Biomater Sci Eng*. 2020;6(5):2726–2739. doi:10.1021/acsbomaterials.9b01987
20. Cochran DL, Jackson JM, Bernard JP, et al. A 5-year prospective multicenter study of early loaded titanium implants with a sandblasted and acid-etched surface. *Int J Oral Maxillofac Implants*. 2011;26(6):1324–1332.
21. Hotchkiss KM, Ayad NB, Hyzy SL, Boyan BD, Olivares-Navarrete R. Dental implant surface chemistry and energy alter macrophage activation in vitro. *Clin Oral Implants Res*. 2017;28(4):414–423. doi:10.1111/clr.12814
22. Yang Y, Wang X, Miron RJ, Zhang X. The interactions of dendritic cells with osteoblasts on titanium surfaces: an in vitro investigation. *Clin Oral Investig*. 2019;23(11):4133–4143. doi:10.1007/s00784-019-02852-w
23. Hotchkiss KM, Reddy GB, Hyzy SL, Schwartz Z, Boyan BD, Olivares-Navarrete R. Titanium surface characteristics, including topography and wettability, alter macrophage activation. *Acta Biomater*. 2016;31:425–434. doi:10.1016/j.actbio.2015.12.003
24. Hamlet SM, Lee RSB, Moon HJ, Alfarsi MA, Ivanovski S. Hydrophilic titanium surface-induced macrophage modulation promotes pro-osteogenic signalling. *Clin Oral Implants Res*. 2019;30(11):1085–1096. doi:10.1111/clr.13522
25. Tan F, Naciri M, Al-Rubeai M. Osteoconductivity and growth factor production by MG63 osteoblastic cells on bioglass-coated orthopedic implants. *Biotechnol Bioeng*. 2011;108(2):454–464. doi:10.1002/bit.22955
26. Kwon YS, Park JW. Osteogenic differentiation of mesenchymal stem cells modulated by a chemically modified super-hydrophilic titanium implant surface. *J Biomater Appl*. 2018;33(2):205–215. doi:10.1177/0885328218786873
27. Ma QL, Zhao LZ, Liu RR, et al. Improved implant osseointegration of a nanostructured titanium surface via mediation of macrophage polarization. *Biomaterials*. 2014;35(37):9853–9867. doi:10.1016/j.biomaterials.2014.08.025
28. Bai L, Chen P, Zhao Y, et al. A micro/nano-biomimetic coating on titanium orchestrates osteo/angio-genesis and osteoimmunomodulation for advanced osseointegration. *Biomaterials*. 2021;278:121162. doi:10.1016/j.biomaterials.2021.121162
29. Yang Y, Zhang T, Jiang M, Yin X, Luo X, Sun H. Effect of the immune responses induced by implants in a integrated three-dimensional micro-nano topography on osseointegration. *J Biomed Mater Res A*. 2021;109(8):1429–1440. doi:10.1002/jbm.a.37134
30. Ren B, Wan Y, Liu C, et al. Improved osseointegration of 3D printed Ti-6Al-4V implant with a hierarchical micro/nano surface topography: an in vitro and in vivo study. *Mater Sci Eng C Mater Biol Appl*. 2021;118:111505. doi:10.1016/j.msec.2020.111505

31. Wang Q, Zhou P, Liu S, et al. Multi-scale surface treatments of titanium implants for rapid osseointegration: a review. *Nanomaterials*. 2020;10(6):1244. doi:10.3390/nano10061244
32. Pearson RM, Casey LM, Hughes KR, Miller SD, Shea LD. In vivo reprogramming of immune cells: technologies for induction of antigen-specific tolerance. *Adv Drug Deliv Rev*. 2017;114:240–255. doi:10.1016/j.addr.2017.04.005
33. Kulangara K, Leong KW. Substrate topography shapes cell function. *Soft Matter*. 2009;5(21):4072–4076. doi:10.1039/b910132m
34. Bettinger C, Langer R, Borenstein J. Engineering substrate micro and nanotopography to control cell function. *Angew Chem*. 2009;48:5406–5415. doi:10.1002/anie.200805179
35. Zheng H, Tian Y, Gao Q, et al. Hierarchical micro-nano topography promotes cell adhesion and osteogenic differentiation via integrin  $\alpha$ 2-PI3K-AKT signaling axis. *Front Bioeng Biotechnol*. 2020;8:463. doi:10.3389/fbioe.2020.00463
36. Seo CH, Furukawa K, Montagne K, Jeong H, Ushida T. The effect of substrate microtopography on focal adhesion maturation and actin organization via the RhoA/ROCK pathway. *Biomaterials*. 2011;32(36):9568–9575. doi:10.1016/j.biomaterials.2011.08.077
37. Changede R, Cai H, Wind SJ, Sheetz MP. Integrin nanoclusters can bridge thin matrix fibres to form cell-matrix adhesions. *Nat Mater*. 2019;18(12):1366–1375. doi:10.1038/s41563-019-0460-y
38. Coxon A, Rieu P, Barkalow FJ, et al. A novel role for the beta 2 integrin CD11b/CD18 in neutrophil apoptosis: a homeostatic mechanism in inflammation. *Immunity*. 1996;5(6):653–666. doi:10.1016/S1074-7613(00)80278-2
39. Panni RZ, Herndon JM, Zuo C, et al. Agonism of CD11b reprograms innate immunity to sensitize pancreatic cancer to immunotherapies. *Sci Transl Med*. 2019;11:499. doi:10.1126/scitranslmed.aau9240
40. Schittenhelm L, Hilkens CM, Morrison VL.  $\beta$ (2) integrins as regulators of dendritic cell, monocyte, and macrophage function. *Front Immunol*. 2017;8:1866. doi:10.3389/fimmu.2017.01866
41. Rogers TH, Babensee JE. The role of integrins in the recognition and response of dendritic cells to biomaterials. *Biomaterials*. 2011;32(5):1270–1279. doi:10.1016/j.biomaterials.2010.10.014
42. Mennens SFB, Bolomini-Vittori M, Weiden J, Joosten B, Cambi A, van den Dries K. Substrate stiffness influences phenotype and function of human antigen-presenting dendritic cells. *Sci Rep*. 2017;7(1):17511. doi:10.1038/s41598-017-17787-z
43. Berman AE, Kozlova NI, Morozevich GE. Integrins: structure and signaling. *Biochemistry*. 2003;68(12):1284–1299. doi:10.1023/b:biry.0000011649.03634.74
44. Rigracciolo DC, Santolla MF, Lappano R, et al. Focal adhesion kinase (FAK) activation by estrogens involves GPER in triple-negative breast cancer cells. *J Exp Clin Cancer Res*. 2019;38(1):58. doi:10.1186/s13046-019-1056-8
45. Zhao X, Guan JL. Focal adhesion kinase and its signaling pathways in cell migration and angiogenesis. *Adv Drug Deliv Rev*. 2011;63(8):610–615. doi:10.1016/j.addr.2010.11.001
46. Anderson JM, Rodriguez A, Chang DT. Foreign body reaction to biomaterials. *Semin Immunol*. 2008;20(2):86–100. doi:10.1016/j.smim.2007.11.004
47. Cha BH, Shin SR, Leijten J, et al. Integrin-mediated interactions control macrophage polarization in 3D hydrogels. *Adv Healthc Mater*. 2017;6(21):1700289. doi:10.1002/adhm.201700289
48. Banchereau J, Steinman RM. Dendritic cells and the control of immunity. *Nature*. 1998;392(6673):245–252. doi:10.1038/32588
49. Mantovani A, Biswas SK, Galdiero MR, Sica A, Locati M. Macrophage plasticity and polarization in tissue repair and remodelling. *J Pathol*. 2013;229(2):176–185. doi:10.1002/path.4133
50. Schietinger A, Greenberg PD. Tolerance and exhaustion: defining mechanisms of T cell dysfunction. *Trends Immunol*. 2014;35(2):51–60. doi:10.1016/j.it.2013.10.001
51. Sridharan R, Cavanagh B, Cameron AR, Kelly DJ, O'Brien FJ. Material stiffness influences the polarization state, function and migration mode of macrophages. *Acta Biomater*. 2019;89:47–59. doi:10.1016/j.actbio.2019.02.048
52. Li J, Zhou P, Attarilar S, Shi H. Innovative surface modification procedures to achieve micro/nano-graded ti-based biomedical alloys and implants. *Coatings*. 2021;11(6):647. doi:10.3390/coatings11060647
53. Kane R, Ma PX. Mimicking the nanostructure of bone matrix to regenerate bone. *Mater Today*. 2013;16(11):418–423. doi:10.1016/j.mattod.2013.11.001
54. Wang F, Shi L, He W-X, et al. Bioinspired micro/nano fabrication on dental implant–bone interface. *Appl Surf Sci*. 2013;265:480–488. doi:10.1016/j.apsusc.2012.11.032
55. Souza JCM, Sordi MB, Kanazawa M, et al. Nano-scale modification of titanium implant surfaces to enhance osseointegration. *Acta Biomater*. 2019;94:112–131. doi:10.1016/j.actbio.2019.05.045
56. Holzwarth JM, Ma PX. Biomimetic nanofibrous scaffolds for bone tissue engineering. *Biomaterials*. 2011;32(36):9622–9629. doi:10.1016/j.biomaterials.2011.09.009
57. Zhao L, Liu L, Wu Z, Zhang Y, Chu PK. Effects of micropitted/nanotubular titania topographies on bone mesenchymal stem cell osteogenic differentiation. *Biomaterials*. 2012;33(9):2629–2641. doi:10.1016/j.biomaterials.2011.12.024
58. Bai L, Zhao Y, Chen P, et al. Targeting early healing phase with titania nanotube arrays on tunable diameters to accelerate bone regeneration and osseointegration. *Small*. 2021;17(4):e2006287. doi:10.1002/smll.202006287
59. Tiainen L, Abreu P, Buciumeanu M, et al. Novel laser surface texturing for improved primary stability of titanium implants. *J Mech Behav Biomed Mater*. 2019;98:26–39. doi:10.1016/j.jmbm.2019.04.052
60. Zhuang LF, Jiang HH, Qiao SC, et al. The roles of extracellular signal-regulated kinase 1/2 pathway in regulating osteogenic differentiation of murine preosteoblasts MC3T3-E1 cells on roughened titanium surfaces. *J Biomed Mater Res A*. 2012;100(1):125–133. doi:10.1002/jbm.a.33247
61. Shiozawa M, Takeuchi H, Akiba Y, et al. Biological reaction control using topography regulation of nanostructured titanium. *Sci Rep*. 2020;10(1):2438. doi:10.1038/s41598-020-59395-4
62. Wang J, Meng F, Song W, et al. Nanostructured titanium regulates osseointegration via influencing macrophage polarization in the osteogenic environment. *Int J Nanomedicine*. 2018;13:4029–4043. doi:10.2147/IJN.S163956
63. Zhuang XM, Zhou B, Ouyang JL, et al. Enhanced MC3T3-E1 preosteoblast response and bone formation on the addition of nano-needle and nano-porous features to microtopographical titanium surfaces. *Biomed Mater*. 2014;9(4):045001. doi:10.1088/1748-6041/9/4/045001

64. Xu R, Hu X, Yu X, et al. Micro-/nano-topography of selective laser melting titanium enhances adhesion and proliferation and regulates adhesion-related gene expressions of human gingival fibroblasts and human gingival epithelial cells. *Int J Nanomedicine*. 2018;13:5045–5057. doi:10.2147/IJN.S166661
65. Nishiguchi S, Kato H, Fujita H, et al. Titanium metals form direct bonding to bone after alkali and heat treatments. *Biomaterials*. 2001;22(18):2525–2533. doi:10.1016/S0142-9612(00)00443-9
66. Rosa MB, Albrektsson T, Francischone CE, Schwartz Filho HO, Wennerberg A. The influence of surface treatment on the implant roughness pattern. *J Appl Oral Sci*. 2012;20(5):550–555. doi:10.1590/S1678-77572012000500010
67. Bayati MR, Molaei R, Kajbafvala A, Zanganeh S, Zargar HR, Janghorban K. Investigation on hydrophilicity of micro-arc oxidized TiO<sub>2</sub> nano/micro-porous layers. *Electrochim Acta*. 2010;55(20):5786–5792. doi:10.1016/j.electacta.2010.05.021
68. Li X, Huang Q, Elkhooly TA, et al. Effects of titanium surface roughness on the mediation of osteogenesis via modulating the immune response of macrophages. *Biomed Mater*. 2018;13(4):045013. doi:10.1088/1748-605X/aabe33
69. Yang Y, Lin Y, Zhang Z, Xu R, Yu X, Deng F. Micro/nano-net guides M2-pattern macrophage cytoskeleton distribution via Src-ROCK signalling for enhanced angiogenesis. *Biomater Sci*. 2021;9(9):3334–3347. doi:10.1039/D1BM00116G
70. Kou PM, Schwartz Z, Boyan BD, Babensee JE. Dendritic cell responses to surface properties of clinical titanium surfaces. *Acta Biomater*. 2011;7(3):1354–1363. doi:10.1016/j.actbio.2010.10.020
71. Cai K, Bossert J, Jandt KD. Does the nanometre scale topography of titanium influence protein adsorption and cell proliferation? *Colloids Surf B Biointerfaces*. 2006;49(2):136–144. doi:10.1016/j.colsurfb.2006.02.016
72. Yokose S, Klokkevold PR, Takei HH, et al. Effects of surface microtopography of titanium disks on cell proliferation and differentiation of osteoblast-like cells isolated from rat calvariae. *Dent Mater J*. 2018;37(2):272–277. doi:10.4012/dmj.2017-036
73. Giannini M, Primerano C, Berger L, et al. Nano-topography: quicksand for cell cycle progression? *Nanomedicine*. 2018;14(8):2656–2665. doi:10.1016/j.nano.2018.07.002
74. Zhang Z, Li Y, He P, et al. Nanotube-decorated hierarchical tantalum scaffold promoted early osseointegration. *Nanomedicine*. 2021;35:102390. doi:10.1016/j.nano.2021.102390
75. Kaneko F, Bang D, Direskeneli RH, Ohno S, Ishigatsubo Y. Immune reactions in Behçet's disease. *Genet Res Int*. 2014;2014:985689. doi:10.1155/2014/985689
76. Morante-Palacios O, Fondelli F, Ballestar E, Martínez-Cáceres EM. Tolerogenic dendritic cells in autoimmunity and inflammatory diseases. *Trends Immunol*. 2021;42(1):59–75. doi:10.1016/j.it.2020.11.001
77. Ioshima K, Ueno T, Arai Y, et al. The change of surface charge by lithium ion coating enhances protein adsorption on titanium. *J Mech Behav Biomed Mater*. 2019;100:103393. doi:10.1016/j.jmbbm.2019.103393
78. Zhang R, Wu H, Ni J, et al. Guided proliferation and bone-forming functionality on highly ordered large diameter TiO<sub>2</sub> nanotube arrays. *Mater Sci Eng C Mater Biol Appl*. 2015;53:272–279. doi:10.1016/j.msec.2015.04.046
79. Fraioli R, Rechenmacher F, Neubauer S, et al. Mimicking bone extracellular matrix: integrin-binding peptidomimetics enhance osteoblast-like cells adhesion, proliferation, and differentiation on titanium. *Colloids Surf B Biointerfaces*. 2015;128:191–200. doi:10.1016/j.colsurfb.2014.12.057
80. Brunetti V, Maiorano G, Rizzello L, et al. Neurons sense nanoscale roughness with nanometer sensitivity. *Proc Natl Acad Sci USA*. 2010;107(14):6264–6269. doi:10.1073/pnas.0914456107
81. Chang DT, Colton E, Matsuda T, Anderson JM. Lymphocyte adhesion and interactions with biomaterial adherent macrophages and foreign body giant cells. *J Biomed Mater Res A*. 2009;91(4):1210–1220. doi:10.1002/jbm.a.32218
82. Zheng X, Zhou F, Gu Y, Duan X, Mo A. Effect of different titanium surfaces on maturation of murine bone marrow-derived dendritic cells. *Sci Rep*. 2017;7:41945. doi:10.1038/srep41945
83. Luu TU, Gott SC, Woo BW, Rao MP, Liu WF. Micro- and nanopatterned topographical cues for regulating macrophage cell shape and phenotype. *ACS Appl Mater Interfaces*. 2015;7(51):28665–28672. doi:10.1021/acsami.5b10589
84. Serrels B, Sandilands E, Serrels A, et al. A complex between FAK, RACK1, and PDE4D5 controls spreading initiation and cancer cell polarity. *Curr Biol*. 2010;20(12):1086–1092. doi:10.1016/j.cub.2010.04.042
85. Wu X, Li S, Wang K, et al. TNF- $\alpha$  regulates ITG $\beta$ 1 and SYND4 expression in nucleus pulposus cells: activation of FAK/PI3K signaling. *Inflammation*. 2019;42(5):1575–1584. doi:10.1007/s10753-019-01019-9
86. Li R, Zou X, Huang H, et al. HMGB1/PI3K/Akt/mTOR signaling participates in the pathological process of acute lung injury by regulating the maturation and function of dendritic cells. *Front Immunol*. 2020;11:1104. doi:10.3389/fimmu.2020.01104
87. Zhang H, Yang S, Masako N, Lee DJ, Cooper LF, Ko CC. Proliferation of preosteoblasts on TiO<sub>2</sub> nanotubes is FAK/RhoA related. *RSC Adv*. 2015;5(48):38117–38124. doi:10.1039/C4RA16803H
88. Shen X, Yu Y, Ma P, et al. Titania nanotubes promote osteogenesis via mediating crosstalk between macrophages and MSCs under oxidative stress. *Colloids Surf B Biointerfaces*. 2019;180:39–48. doi:10.1016/j.colsurfb.2019.04.033
89. Hochrein H, Shortman K, Vremec D, Scott B, Hertzog P, O'Keefe M. Differential production of IL-12, IFN- $\alpha$ , and IFN- $\gamma$  by mouse dendritic cell subsets. *J Immunol*. 2001;166(9):5448–5455. doi:10.4049/jimmunol.166.9.5448
90. Wolenski M, Cramer SO, Ehrlich S, et al. Expression of CD83 in the murine immune system. *Med Microbiol Immunol*. 2003;192(4):189–192. doi:10.1007/s00430-003-0179-9
91. Ma X, Trinchieri G. Regulation of interleukin-12 production in antigen-presenting cells. *Adv Immunol*. 2001;79:55–92.
92. O'Shea JJ, Paul WE. Regulation of T(H)1 differentiation—controlling the controllers. *Nat Immunol*. 2002;3(6):506–508. doi:10.1038/ni0602-506
93. Watford WT, Moriguchi M, Morinobu A, O'Shea JJ. The biology of IL-12: coordinating innate and adaptive immune responses. *Cytokine Growth Factor Rev*. 2003;14(5):361–368. doi:10.1016/S1359-6101(03)00043-1
94. Shu T, Zhang Y, Sun G, et al. Enhanced osseointegration by the hierarchical micro-nano topography on selective laser melting Ti-6Al-4V dental implants. *Front Bioeng Biotechnol*. 2020;8:621601. doi:10.3389/fbioe.2020.621601

International Journal of Nanomedicine

Dovepress

## Publish your work in this journal

The International Journal of Nanomedicine is an international, peer-reviewed journal focusing on the application of nanotechnology in diagnostics, therapeutics, and drug delivery systems throughout the biomedical field. This journal is indexed on PubMed Central, MedLine, CAS, SciSearch<sup>®</sup>, Current Contents<sup>®</sup>/Clinical Medicine, Journal Citation Reports/Science Edition, EMBase, Scopus and the Elsevier Bibliographic databases. The manuscript management system is completely online and includes a very quick and fair peer-review system, which is all easy to use. Visit <http://www.dovepress.com/testimonials.php> to read real quotes from published authors.

Submit your manuscript here: <https://www.dovepress.com/international-journal-of-nanomedicine-journal>